Electronic Supplementary Material (ESI) for Journal of Materials Chemistry A.
This journal is © The Royal Society of Chemistry 2022

Supporting Information

Novel 2D porous C_3N_2 framework as promising anode material with ultra-high specific capacity for lithium-ion batteries

Xinyong Cai,[a, 1] Wencai Yi,[b, 1] Jiao Chen,[a] Linguo Lu,[c] Bai Sun,[a] Yuxiang Ni,[a] Simon A. T. Redfern,[d,*] Hongyan Wang,[a] Zhongfang Chen,[c,*] Yuanzheng Chen [a, e, f, *]

[a] *School of Physical Science and Technology, Southwest Jiaotong University, Chengdu 610031, China*

[b] *Laboratory of High Pressure Physics and Material Science (HPPMS), School of Physics and Physical Engineering, Qufu Normal University, Qufu, Shandong, 273165, China.*

[c] *Department of Chemistry, University of Puerto Rico, Rio Piedras Campus, San Juan, PR 00931, USA*

[d] *Asian School of the Environment and School of Materials Science and Engineering, Nanyang Technological University, Singapore, 639798, Singapore*

[e] *Beijing Computational Science Research Center, Haidian District, Beijing 100193, China*

[f] *Department of Physics and Centre for Advanced Two-Dimensional Materials, National University of Singapore, Singapore, 117551, Singapore*

[1] *Authors equally contribute to this work.*

**Email: (S. A. T. R.) simon.redfern@ntu.edu.sg; (Z. C.) zhongfangchen@gmail.com; (Y. C.) cyz@swjtu.edu.cn*

Index

page

Computational Details

The local structural relaxations and electronic properties calculations were performed in the framework of the density functional theory (DFT) within the generalized gradient approximation (GGA) parametrized as implemented in the VASP code.[1] The $2s^22p^2$, $2s^22p^3$, and $3s^1$ atomic orbitals were treated as valence states for C, N, and Li, respectively. The cut-off energy for the expansion of wavefunctions into plane waves was set to 500 eV in all the calculations. The vacuum region of 20 Å was inserted between adjacent images in *z* direction in order to avoid the interactions between neighboring layers. The convergence thresholds were set as 1.0×10^{-6} for total energy and 1 meV/Å for atomic force. The Brillouin zone was sampled with the resolution of $0.03 \times 2\pi$ Å^{-1} with *k* points mesh. Van der Waals's interactions were taken into account using the semiempirical DFT-D2 and DFT-D3 approaches.

The cohesive energy of the PCGN monolayers was calculated by using the following formula:

$$E_{coh} = (E_{C_xN_y} - xE_C - yE_N)/(x + y) \quad (1)$$

The adsorption energy (E_{ad}) of the Li atom on the α-C_xN_y monolayer was obtained by

$$E_{ad} = (E_{Li_nC_xN_y} - nE_{Li} - E_{C_xN_y})/n \quad (2)$$

where E_N, E_C, E_{Li}, $E_{C_xN_y}$, and $E_{Li_nC_xN_y}$ are the total energies of a single N atom, a single C atom, a Li atom in body-centered cubic (bcc) structure, one unit cell of the α-C_xN_y monolayer, and the lithiated monolayer, respectively. The specific capacity (*C*) was calculated following the formula

$$C = \frac{n}{m} * \frac{F}{M} \quad (3)$$

where F, M, n, stand for the Faraday constant (26.8 Ah mol^{-1}) and the molar mass (e.g., 64 g mol^{-1} for α-C_3N_2), and the number of Li-ion during the lithiation for $(C_3N_2)_mLi_n$, respectively,

and m is 6 for the unit cell of α-C_3N_2.

Phonon dispersion calculations were carried out for the supercell with over 96 atoms (e.g., a 2 ×2 supercell for α-C_3N_2), which was based on the supercell approach as done in the Phonopy code.[2] First-principles molecular dynamics (MD) simulations for three supercells were performed at different temperatures of 500, 750 and 1000 K. MD simulation in the NVT ensemble lasted for 12 ps with a time step of 2.0 fs. The temperature was controlled by using the Nosé-Hoover method. The climbing image nudged elastic band (CI-NEB) method was employed to calculate the diffusion barriers of the Li atoms.

Supplementary Note 1:

The low-energy 2D C-N structures by PSO structure search

The particle swarm optimization (PSO) method within the evolutionary algorithm as implemented in the Crystal structure AnaLYsis by Particle Swarm Optimization (PSO) code was employed to find the lowest energy structures of C_xN_y (x,y = 1, 2, 3, 4, 5, and 6) monolayers.[3, 4] Unit cells containing 1, 2, 3, 4, 5, and 6 formula units (f.u.) were considered. In the first step, random structures with certain symmetry are constructed in which atomic coordinates are generated by the crystallographic symmetry operations. Local optimizations using the VASP code [5] were done with the conjugate gradients method and stopped when Gibbs free energy changes became smaller than 1×10^{-5} eV per cell. After processing the first-generation structures, 60% of structures with lower Gibbs free energies are selected to construct the next generation structures by PSO. 40% of the structures in the new generation are randomly generated. A structure fingerprinting technique of bond characterization matrix is applied to the generated structures, so that identical structures are strictly forbidden. These procedures significantly enhance the diversity of the structures, which is crucial for structural global search efficiency. Structural searching for

each calculation was stopped after generating 1000 ~ 1200 structures (e.g., about 20 ~ 30 generations).

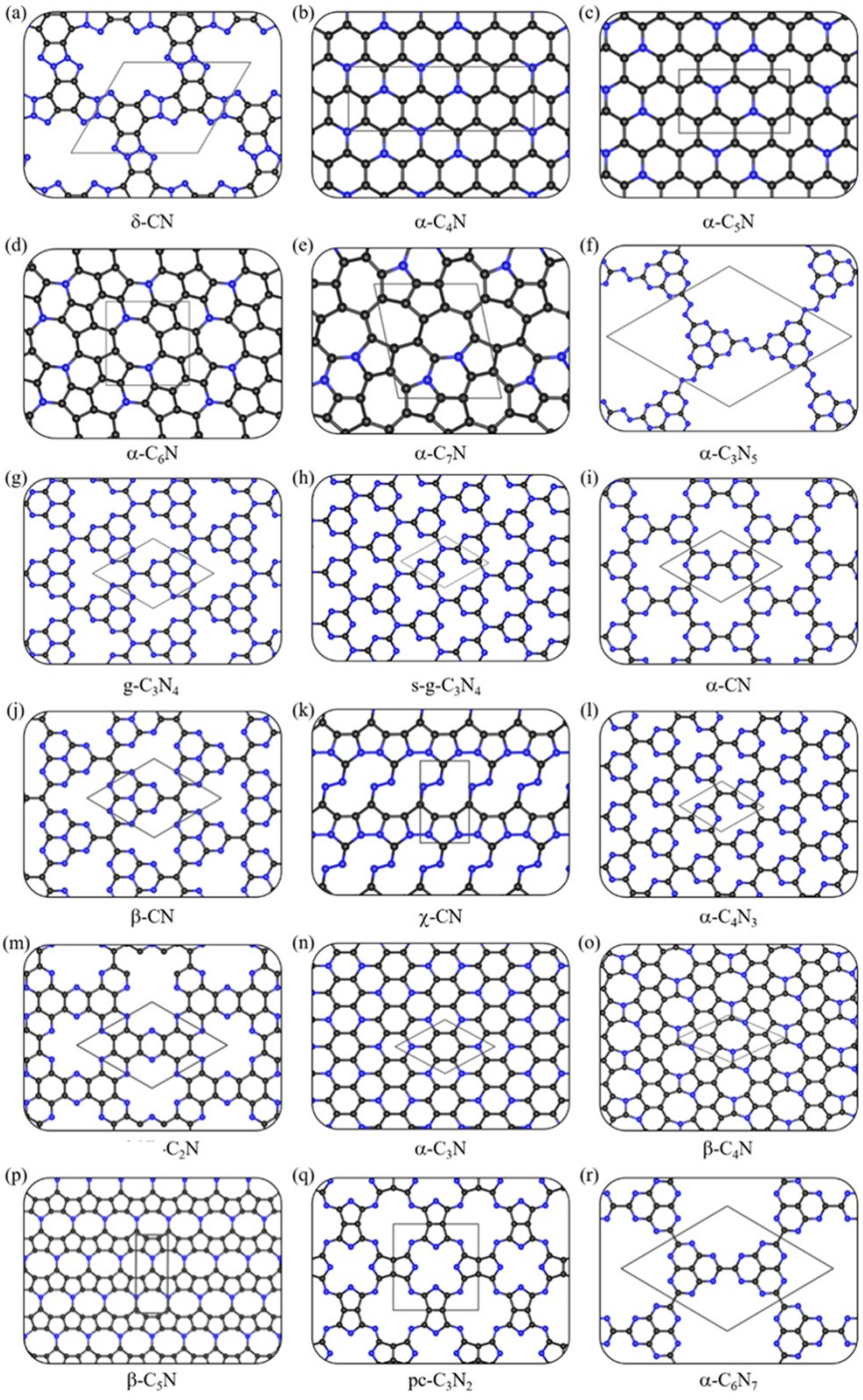

The above presents some low-energy structures at different stoichiometry ratios (including our predicted structures and the reported structures). (a) δ-CN, (b) C_4N, (c) C_5N, (d) C_6N, (e) C_7N, (f) C_3N_5,[6] (g) g-C_3N_4,[7, 8] (h) s-g-C_3N_4,[7, 9] (i) C_3N_3,[10, 11] (j) β-CN,[10] (k) χ-CN,[12] (l) α-C_4N_3,[13] (m) C_2N,[14] (n) C_3N,[15] (o) β-C_4N,[16] (p) β-C_5N,[17] (q) α-C_6N_7,[18] (r) pc-C_3N_2.[19] The black and blue balls represent C and N atoms, respectively.

Supplementary Note 2:

The pore C-N skeletons by assembling organic units

Through the analysis of low-energy porous C-N structures, such as α-C_3N_5, α-CN, C_2N, g-C_3N_4, and s-g-C_3N_4 monolayers, which also have been experimentally synthesized, we found that they mainly originate from symmetric N-rich organic units and few auxiliary C-rich organic units.

Herein, we present some typical organic units in the following (e.g. (a) hexaaminobenzene trihydrochloride,[14] (b) 2, 3, 6, 7, 10, 11-Hexaaminotriphenylene hexahydrochloride,[20-22] (c-f)Triazine,[23, 24] Heptazine,[6, 25] (h)1,4-piperazinedicarboxaldehyde,[26] (i)1,2,4,5-tetraaminobenzene,[20, 27, 28] (j)2,4,6-trichloro-1,3,5-triazine,[10, 29] (k) Phthalocyanine,[19] and (l) Pyrazine [28]) and auxiliary C-rich organic units (e.g. (r)1,4-diformylbenzene[30], (s) benzene-1,3,5-tricarboxylic,[27] (f) hexaketocyclohexane octahydrate,[14, 20, 28]and (u) Benzene).

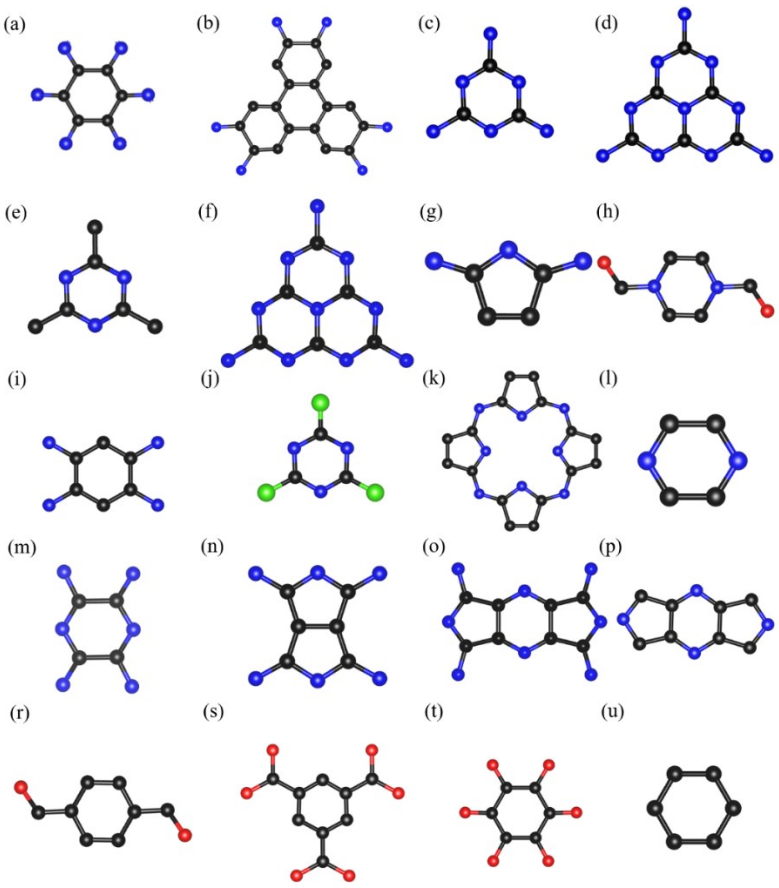

Assembling these organic units by various building block (e.g., knots, linkers) combinations, we can obtain various shapes, sizes, porous C-N skeletons as follows. Topology diagrams showing these pore C-N skeletons with trigon and hexagon uniform pores are given below.

(1) Some synthesized porous C-N sheets:

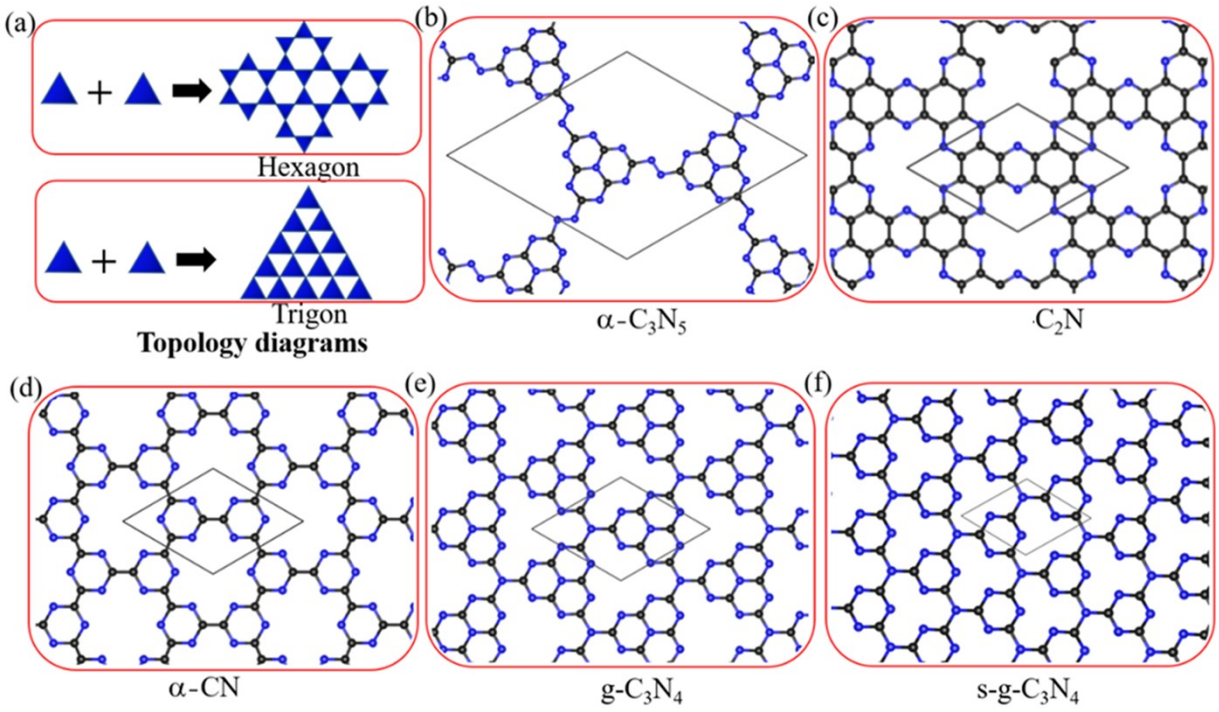

(2) Design some new porous C-N sheets:

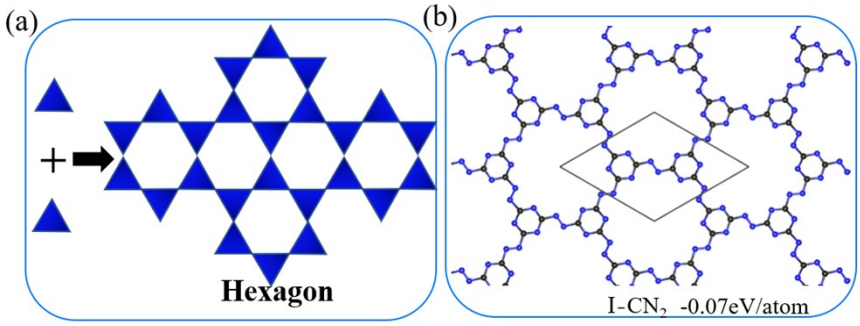

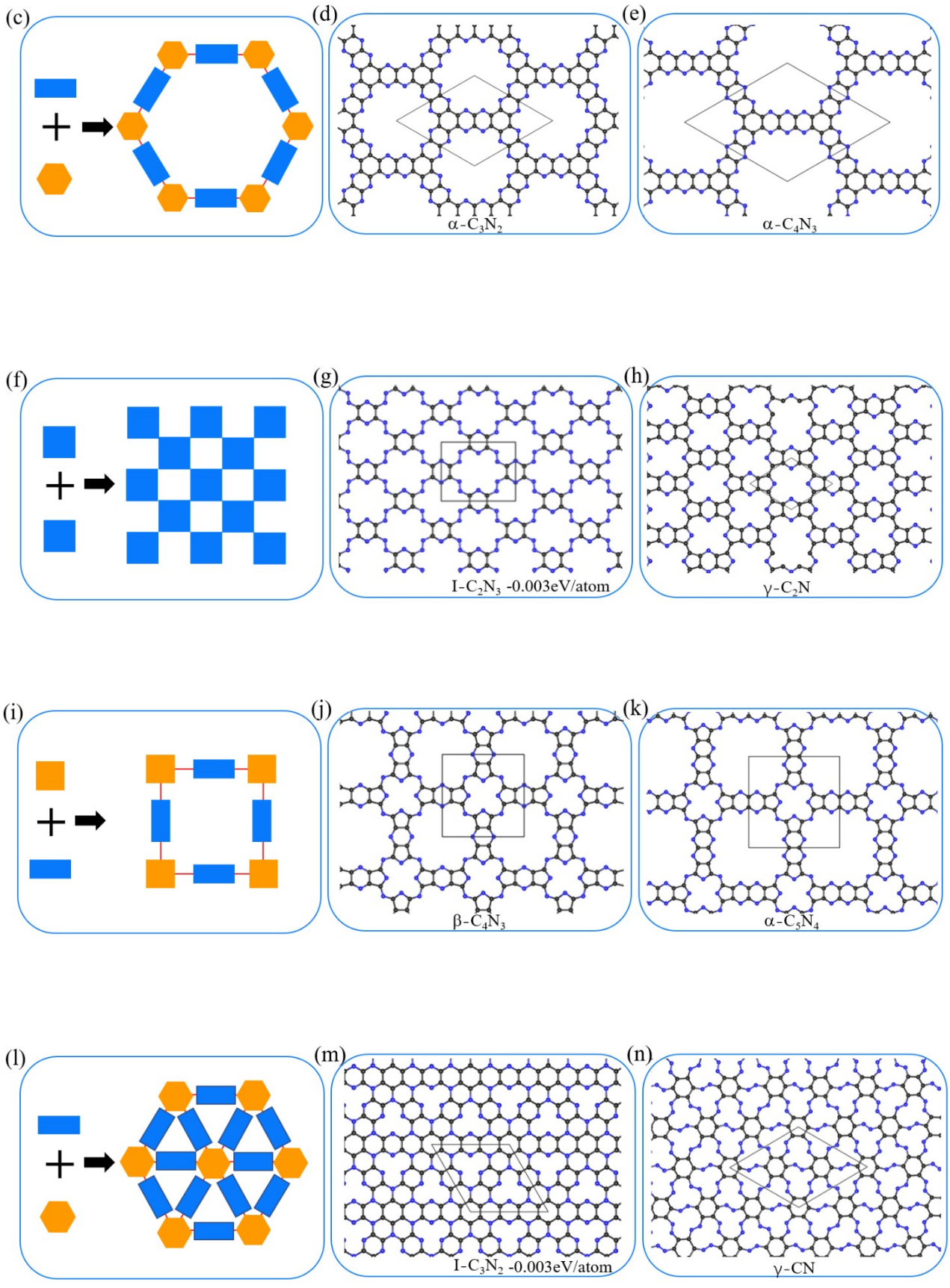
(c)
(d)
α-C3N2
(e)
α-C4N3
(f)
(g)
I-C2N3 -0.003eV/atom
(h)
γ-C2N
(i)
(j)
β-C4N3
(k)
α-C5N4
(l)
(m)
I-C3N2 -0.003eV/atom
(n)
γ-CN

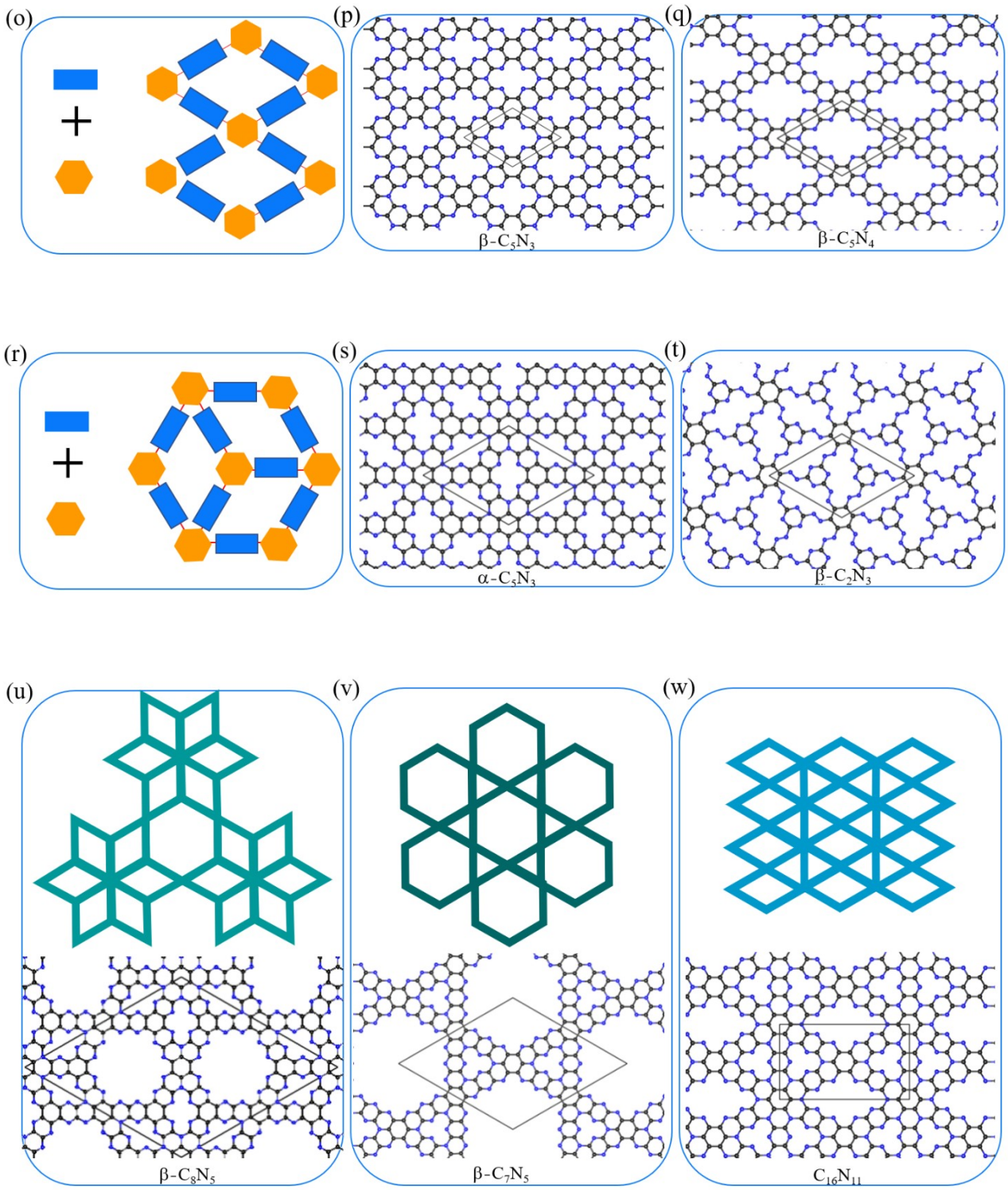
(o)
(p)
β-C5N3
(q)
β-C5N4
(r)
(s)
α-C5N3
(t)
β-C2N3
(u)
β-C8N5
(v)
β-C7N5
(w)
C16N11

Supplementary Note 3:

The extracted pore C-N skeletons from COFs

Some COF_S (e.g. C_2N, g-C_3N_4, and C_3N_5) can lose edge functional groups after being annealed at some temperature, leading to N-rich COFs. However, using such C-N skeletons to construct porous structures has not been attempted, which is a new method we used in this study.

Through our extensive survey, we obtained some porous C-N skeletons. Their optimized geometric structures and phonon spectra are given below. (a) β-C_3N, (b) α-C_5N_2, (c) β-C_5N_2, and (d) β-C_4N from covalent triazine framework (CTF-0),[31] aza-fused π-Conjugated microporous polymers (Aza-CMPs),[32-34] iron phthalocyanine organometallic polymer (poly-FePc),[35] and aza-COF-2,[20-22] respectively.

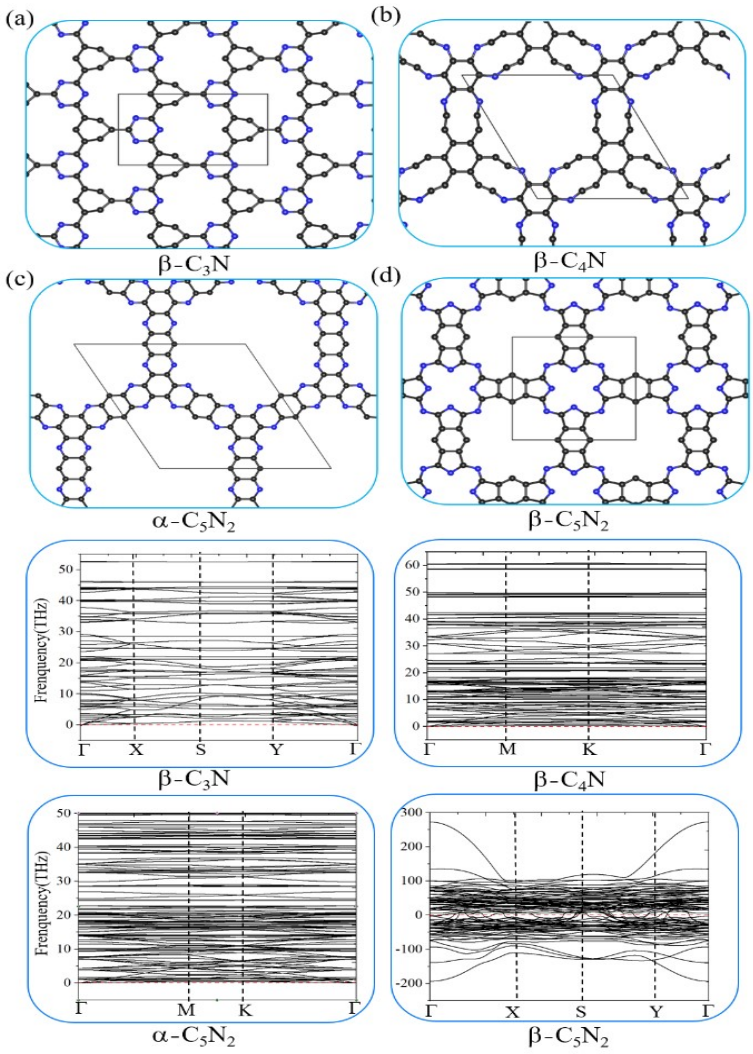
(a)
β-C3N
(b)
β-C4N
(c)
α-C5N2
(d)
β-C5N2
Frenquency(THz)
Γ X S Y Γ
β-C3N
Γ M K Γ
β-C4N
Γ M K Γ
α-C5N2
Γ X S Y Γ
β-C5N2

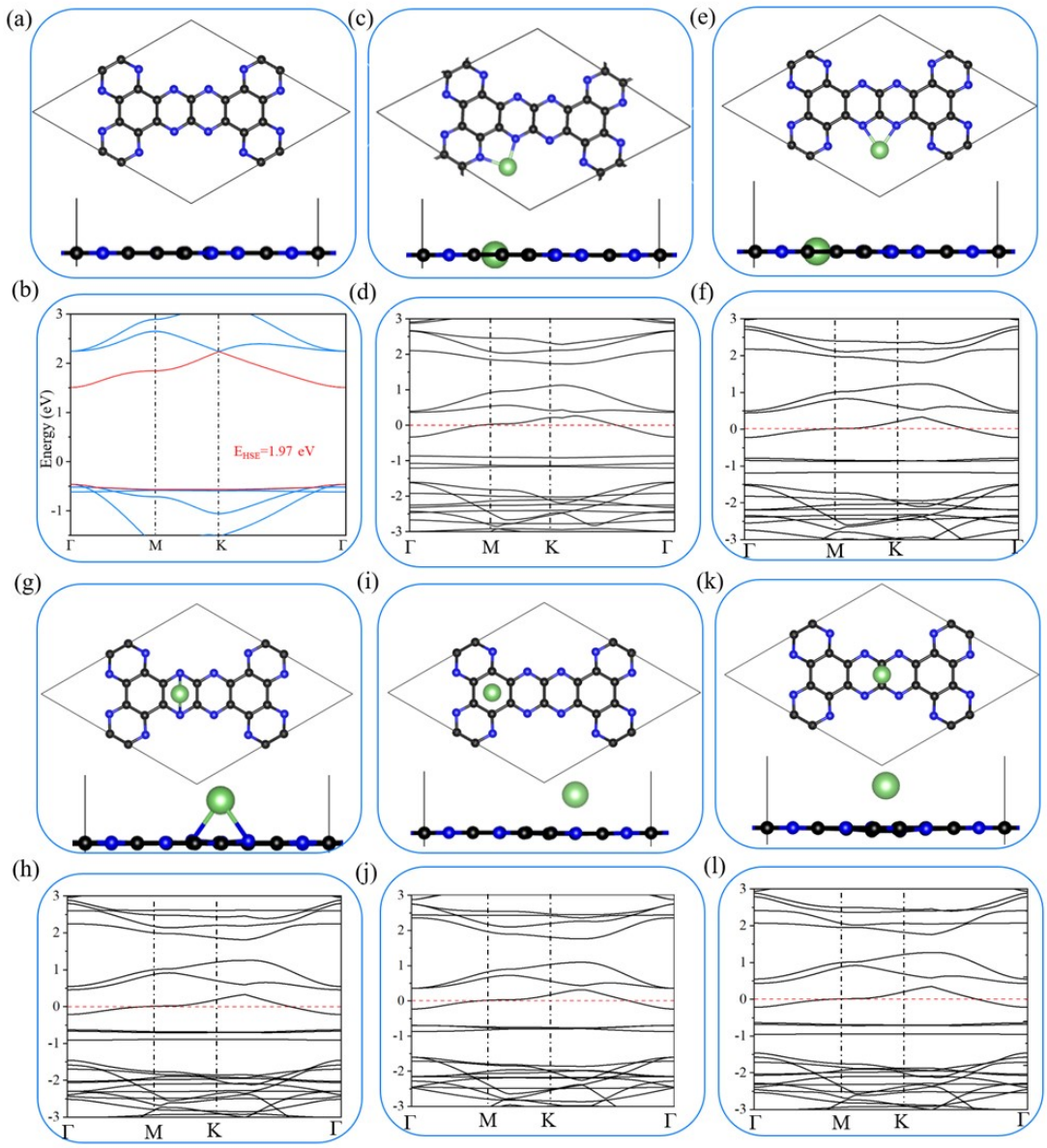

Figure S1. (a-b) Top and side views, and electronic band structure of pristine α-C_3N_2 monolayer. (c-l) Top and side views, and electronic band structures for α-C_3N_2 monolayer with Li absorbed at different sites.

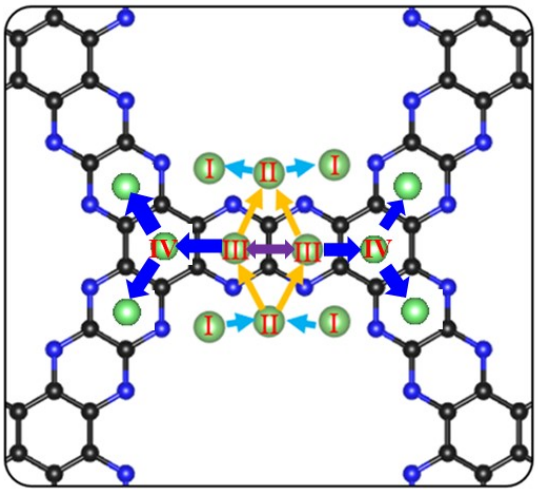

Figure S2. (a) Schematics of the diffusion paths I→II, II→III, III→III, and III→IV in the pristine α-C_3N_2 framework (top view).

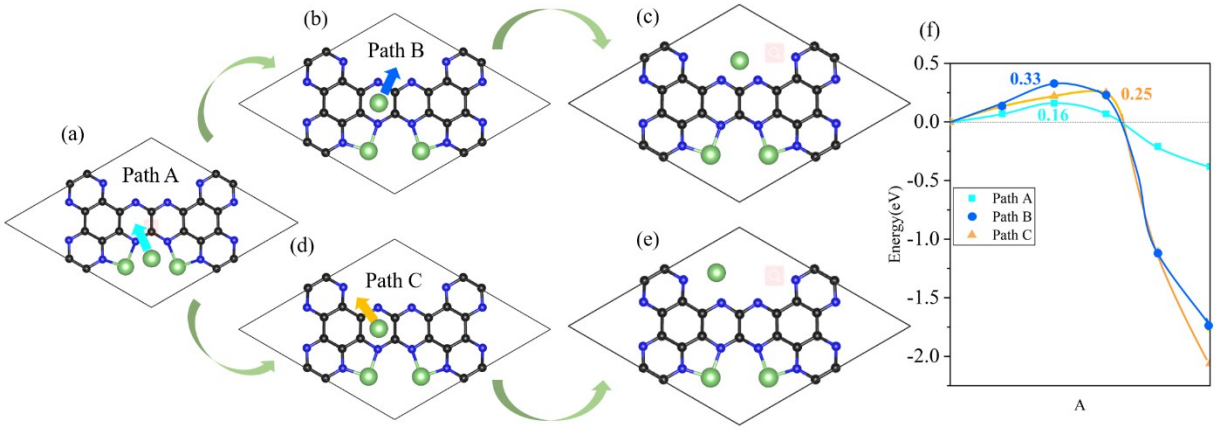

Figure S3. The schematics (a-e) for a configuration of three Li-ions surrounding on the α-C_3N_2 framework and the diffusion of middle Li-ion from one pore to another along different paths (Path A, Path B, Path C) and (f) the calculated ion diffusion barriers.

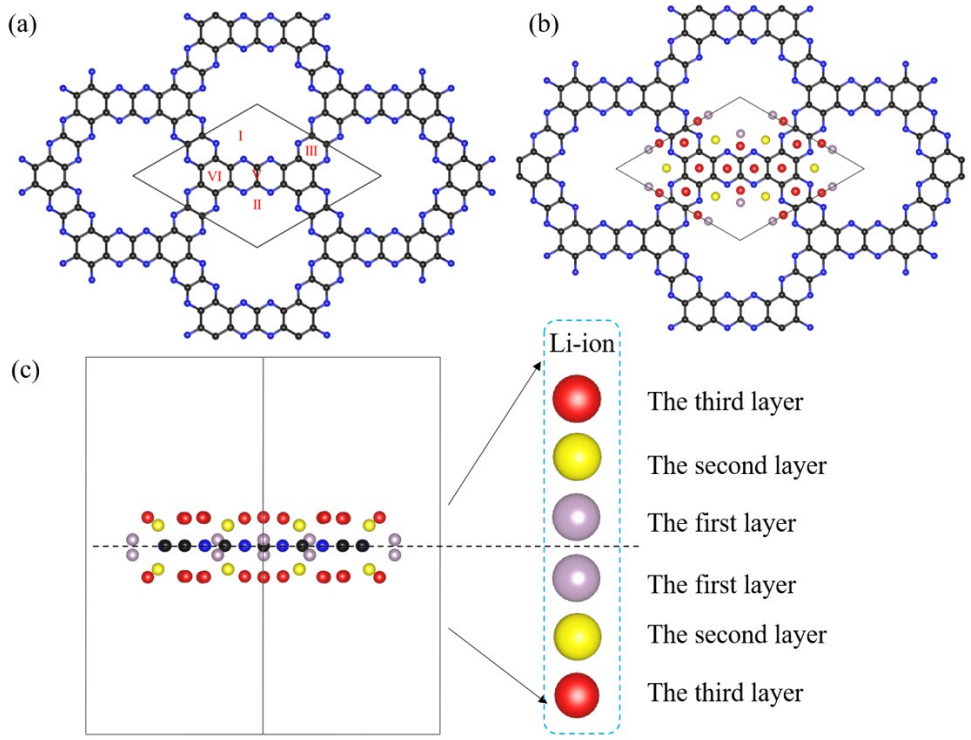

Figure S4. (a) The different Li-adsorption sites in α-C_3N_2 framework. The top (b) and side (c) views of all the possible Li adsorption sites and the multiple-layer Li atom adsorption on both sides of α-C_3N_2 monolayer.

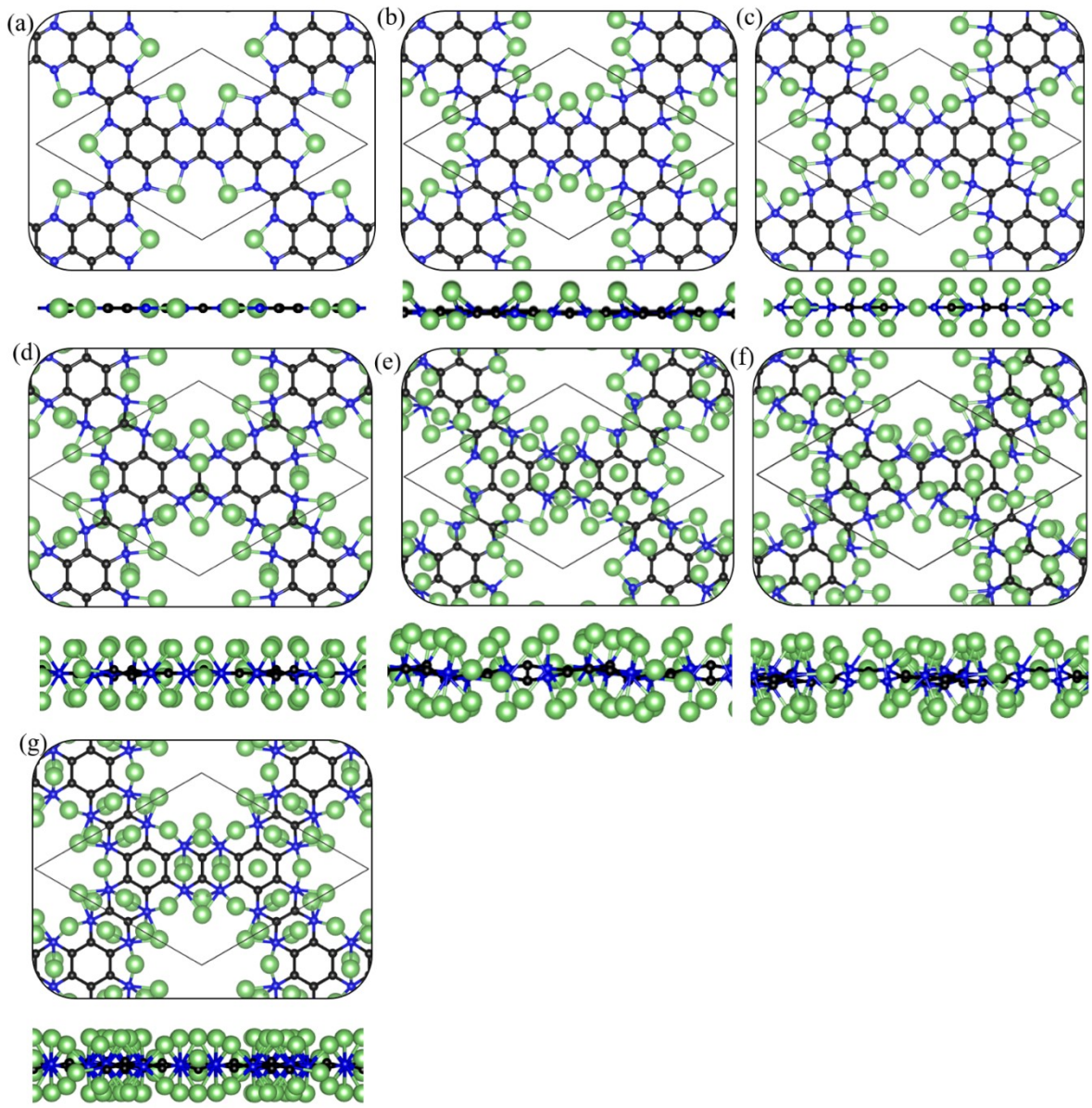

Figure S5. Top and side views of the optimized adsorption configurations at six different Li concentrations for the lithiated α-C_3N_2 monolayer. (a) $(C_3N_2)_6Li_6$, (b) $(C_3N_2)_6Li_{12}$, (c) $(C_3N_2)_6 Li_{18}$, (d) $(C_3N_2)_6Li_{24}$, (e) $(C_3N_2)_6Li_{30}$, (f) $(C_3N_2)_6Li_{36}$, and (g) $(C_3N_2)_6Li_{40}$.

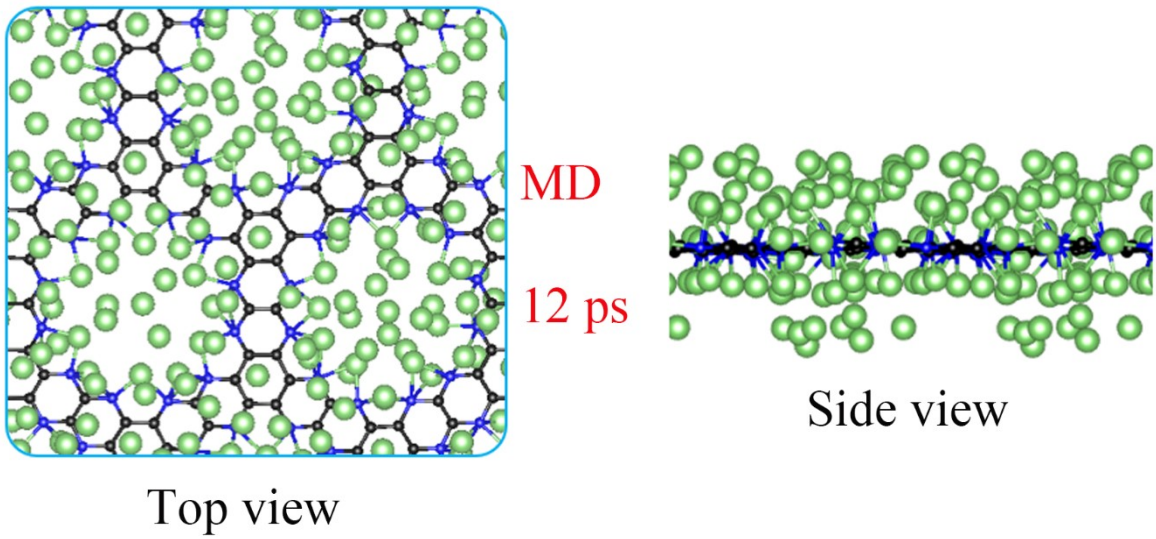

Figure S6. Snapshot after 12 ps MD simulations of $Li_{40}(C_3N_2)_6$ at the temperature of 300 K

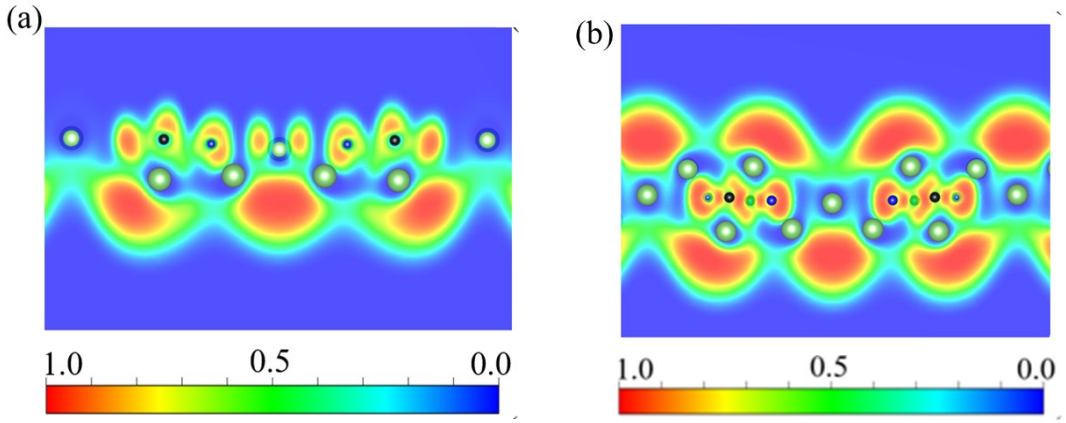

Figure S7. 2D ELF map of lithiated α-C_3N_2 framework with (a) two-layer and (b) three-layer Li atom adsorptions.

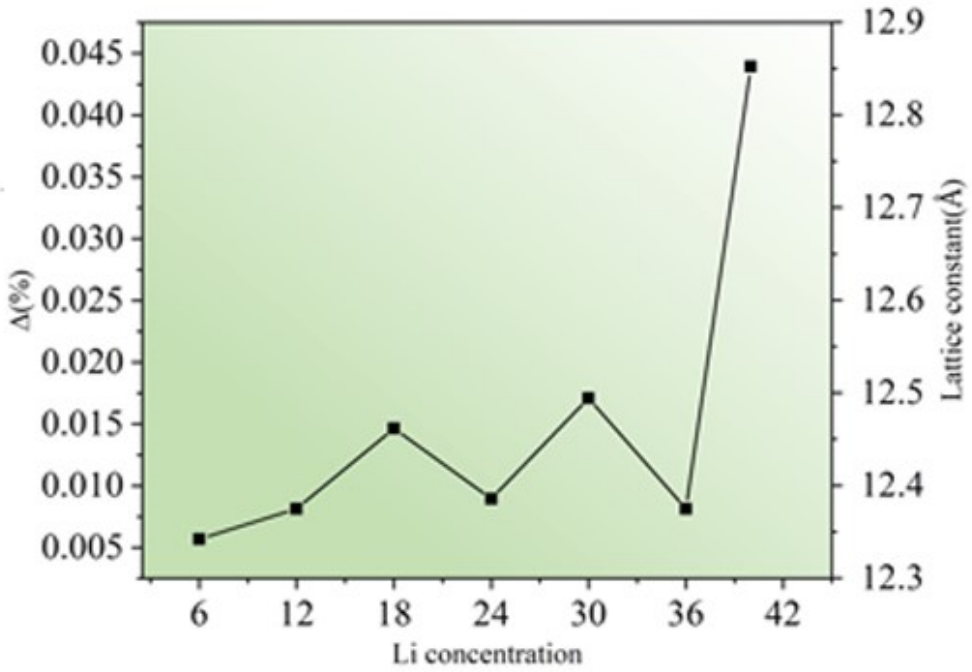

Figure S8. Lattice expansion degree (Δ) and lattice constant vary with the increase of absorbed Li-ions.

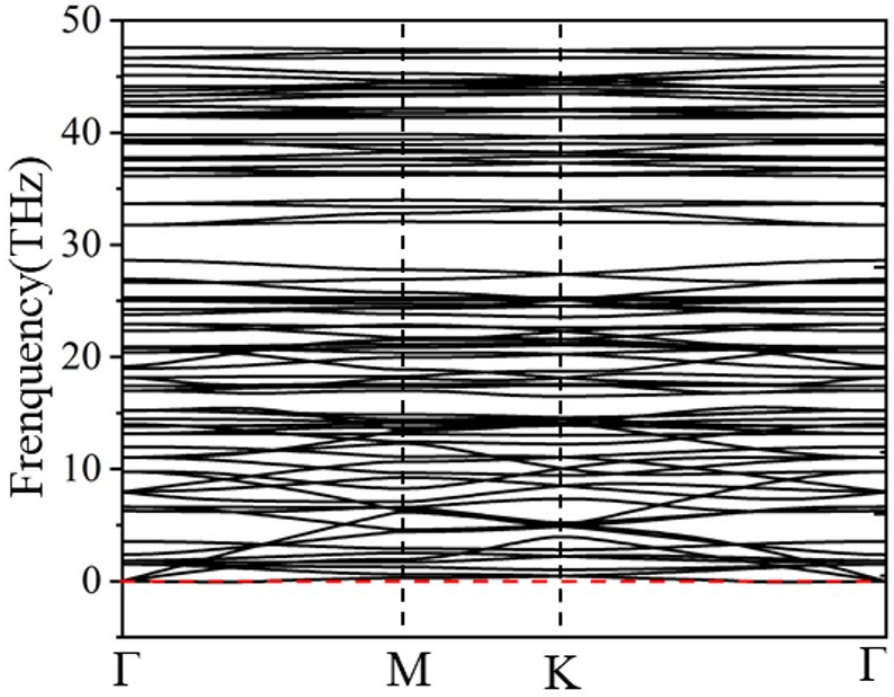

Figure S9. Phonon spectrum of the proposed α-C_3N_2 monolayer.

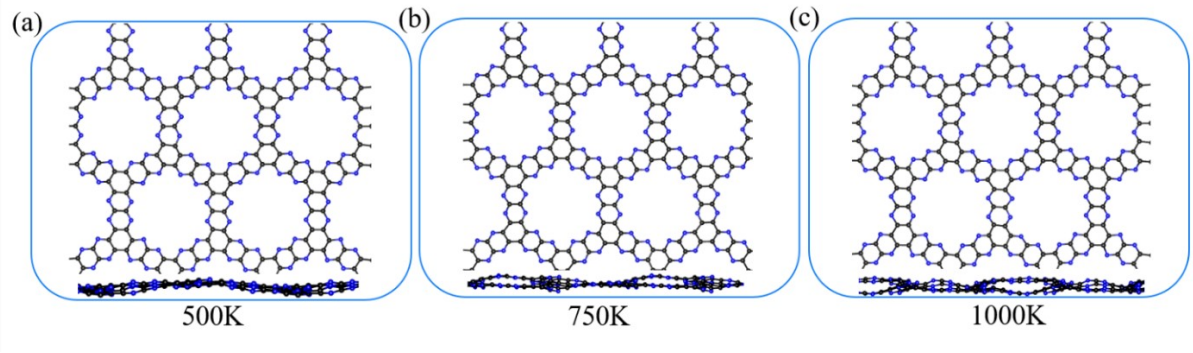

Figure S10. Thermal stability of the α-C_3N_2 monolayer. Snapshots of the final frame of α-C_3N_2 monolayer at temperatures of (b) 500 K, (c) 750 K, and (d) 1000 K at the end of 12 ps MD simulations.

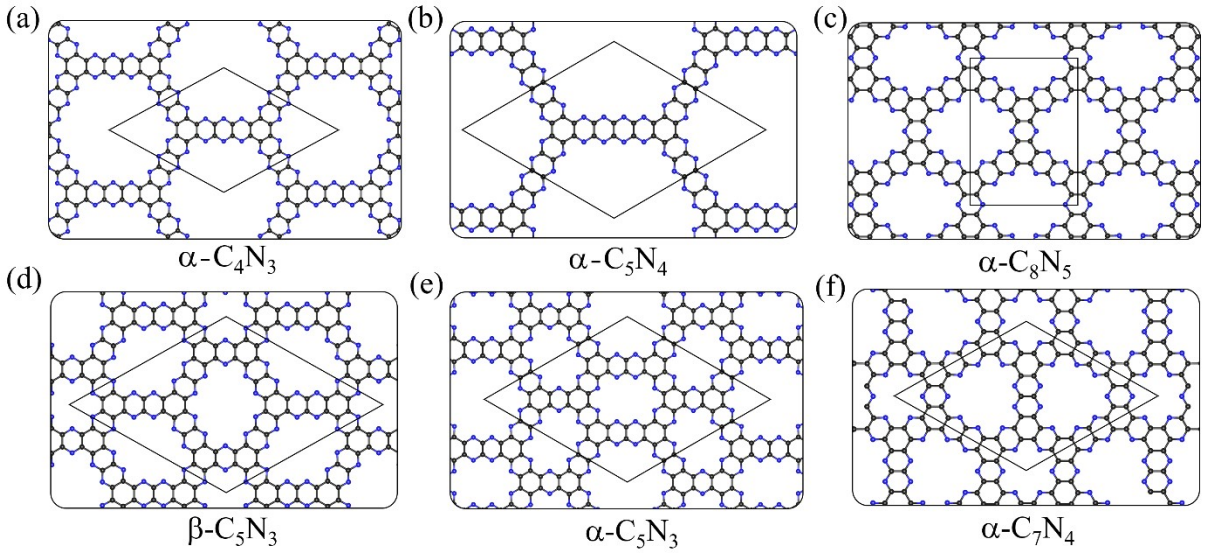

Figure S11. 2D C-N frameworks with different pore sizes and hierarchical porosity obtained by combining building blocks. (a) β-C_3N_2, (b) α-C_4N_3, (c) α-C_5N_4, (d) α-C_8N_5, (e) β-C_5N_3, (f) α-C_5N_3, and (g) α-C_7N_4

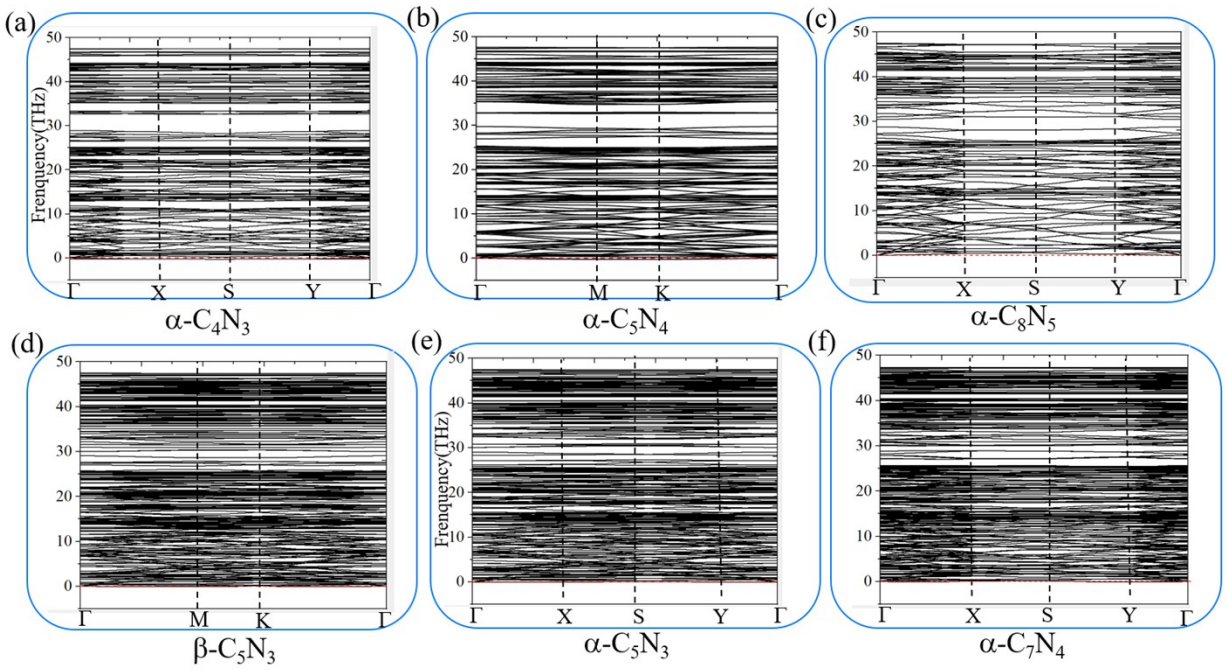

Figure S12. Phonon spectra of the α-C_3N_2 derivatives: (a) β-C_3N_2, (b) α-C_4N_3, (c) α-C_5N_4, (d) α-C_8N_5, (e) β-C_5N_3, (f) α-C_5N_3, and (g) α-C_7N_4 monolayers.

Table S1. Structural information of α-C_3N_2 and other porous C-N monolayers

Phase	Space Group	Lattice Parameters (Å,°)	Atoms	Wyckoff Positions (fractional)		
				x	y	z
α-C_3N_2	P6/mmm	a=12.29	C1	0.214	0.666	0.500
		b=12.29	C2	0.441	0.441	0.500
		c=20	N1	0.108	0.670	0.500
		α=β=90				
		γ=120				
α-C_4N_3	P6/mmm	a=16.26	C1	0.081	0.585	0.500
		b=16.26	C2	0.243	0.666	0.500
		c=20	C3	0.505	0.585	0.500
		α=β=90	N1	0.163	0.669	0.500
		γ=120	N2	0.589	0.589	0.500
α-C_5N_4	P6/mmm	a=20.24	C1	0.130	0.601	0.500
		b=20.24	C2	0.261	0.666	0.500
		c=20	C3	0.464	0.464	0.500
		α=β=90	N1	0.066	0.604	0.500

		γ=120	N2	0.197	0.669	0.500
α-C_8N_5	Cmmm	a=12.28	C1	0.059	0.932	0.500
		b=16.78	C2	0.601	0.781	0.500
		c=20	C3	0.119	0.856	0.500
		α=β=γ=90	C4	0.280	0.787	0.500
			N1	0.227	0.858	0.500
			N2	0.386	0.500	0.500
			N3	0.111	0.711	0.500
β-C_5N_3	P6/mmm	a=20.63	C1	0.865	0.064	0.500
		b=820.63	C2	0.795	0.064	0.500
		c=20	C3	0.795	0.135	0.500
		α=β=90	C4	0.731	0.199	0.500
		γ=120	C5	0.667	0.263	0.500
			N1	0.729	0.133	0.500
			N2	0.665	0.197	0.500
			N3	0.270	0.270	0.500
			N4	0.134	0.134	0.500
β-C_7N_4	Cmmm	a=10.38	C1	0.341	0.836	0.500
		b=10.38	C2	0.033	0.793	0.500
		c=20	C3	0.362	0.987	0.500
		α=β=90	C4	0.913	0.913	0.500
		γ=132.67	N1	0.479	0.852	0.500
			N2	0.768	0.890	0.500
α-C_5N_3	P6/mmm	a=20.63	C1	0.199	0.872	0.500
		b=20.63	C2	0.269	0.872	0.500
		c=40	C3	0.269	0.800	0.500
		α=β=90	C4	0.333	0.737	0.500
		γ=120	C5	0.737	0.737	0.500
			C6	0.667	0.667	0.500
			N1	0.197	0.935	0.500
			N2	0.335	0.935	0.500
			N3	0.334	0.802	0.500

References

1. J. P. Perdew, K. Burke and M. Ernzerhof, *Phys. Rev. Lett.*, 1996, **77**, 3865-3868.

2. A. Togo and I. Tanaka, *Scr. Mater.*, 2015, **108**, 1-5.

3. Y. Wang, J. Lv, L. Zhu and Y. Ma, *Comput. Phys. Commun.*, 2012, **183**, 2063-2070.

4. Y. C. Wang, J. A. Lv, L. Zhu and Y. M. Ma, *Phys. Rev. B*, 2010, **82**, 094116-094123.

5. G. Kresse and J. Furthmüller, *Phys. Rev. B*, 1996, **54**, 11169-11186.

6. P. Kumar, E. Vahidzadeh, U. K. Thakur, P. Kar, K. M. Alam, A. Goswami, N. Mahdi, K. Cui, G. M. Bernard, V. K. Michaelis and K. Shankar, *J. Am. Chem. Soc.*, 2019, **141**, 5415-5436.

7. W. J. Ong, L. L. Tan, Y. H. Ng, S. T. Yong and S. P. Chai, *Chem. Rev.*, 2016, **116**, 7159-7329.

8. K. Kailasam, J. Schmidt, H. Bildirir, G. Zhang, S. Blechert, X. Wang and A. Thomas, *Macromol Rapid Commun.*, 2013, **34**, 1008-1013.

9. X. Zhou, F. Li, Y. Xing and W. Feng, *J. Mater. Chem. C*, 2019, **7**, 3360-3368.

10. A. Wang, X. Zhang and M. Zhao, *Nanoscale*, 2014, **6**, 11157-11162.

11. J. Feng and M. Li, *Adv. Funct. Mater.*, 2020, **30**, 2001502-2001509.

12. T. Li, C. He and W. Zhang, *J. Mater. Chem. A*, 2019, **7**, 4134-4144.

13. A. Du, S. Sanvito and S. C. Smith, *Phys. Rev. Lett.*, 2012, **108**, 197207-1972011.

14. J. Mahmood, E. K. Lee, M. Jung, D. Shin, I. Y. Jeon, S. M. Jung, H. J. Choi, J. M. Seo, S. Y. Bae, S. D. Sohn, N. Park, J. H. Oh, H. J. Shin and J. B. Baek, *Nat. Commun.*, 2015, **6**, 6486-6492.

15. J. Mahmood, E. K. Lee, M. Jung, D. Shin, H. J. Choi, J. M. Seo, S. M. Jung, D. Kim, F. Li, M. S. Lah, N. Park, H. J. Shin, J. H. Oh and J. B. Baek, *Proc. Natl. Acad. Sci. USA*, 2016, **113**, 7414-7419.

16. C. Pu, D. Zhou, Y. Li, H. Liu, Z. Chen, Y. Wang and Y. Ma, *J. Phys. Chem. C*, 2017, **121**, 2669-2674.

17. D. Wang, H. Li, L. Zhang, Z. Sun, D. Han, L. Niu and J. Zhao, *Adv. Theor. Simul.*, 2018, **2**,

1800165-1800171.

18. B. Liu, B. Xu, S. Li, J. Du, Z. Liu and W. Zhong, *J. Mater. Chem. A*, 2019, **7**, 20799.

19. L. Tsetseris, *2D Mater.*, 2016, **3**, 021006-021011.

20. Z. Meng, A. Aykanat and K. A. Mirica, *Chem. Mater.*, 2018, **31**, 819-825.

21. I. Ahmad, F. Li, C. Kim, J.-M. Seo, G. Kim, J. Mahmood, H. Y. Jeong and J.-B. Baek, *Nano Energy*, 2019, **56**, 581-587.

22. L. Meng, S. Ren, C. Ma, Y. Yu, Y. Lou, D. Zhang and Z. Shi, *Chem. Commun.*, 2019, **55**, 9491-9494.

23. L. Lin, Z. Yu and X. Wang, *Angew. Chem. Int. Ed. Engl.*, 2019, **58**, 6164-6175.

24. G. J. Martyna, M. L. Klein and M. Tuckerman, *J. Chem. Phys.*, 1992, **97**, 2635-2643.

25. B. Jürgens, E. Irran, J. Senker, P. Kroll, H. Müller and W. Schnick, *J. Am. Chem. Soc.*, 2003, **125**, 10288-10300.

26. L. Li, F. Lu, R. Xue, B. Ma, Q. Li, N. Wu, H. Liu, W. Yao, H. Guo and W. Yang, *ACS Appl. Mater. Inter.*, 2019, **11**, 26355-26363.

27. S.-Y. Bae, D. H. Kweon, J. Mahmood, M.-J. Kim, S.-Y. Yu, S.-M. Jung, S.-H. Shin, M. J. Ju and J.-B. Baek, *Nano Energy*, 2017, **34**, 533-540.

28. C. Ma, X. Li, J. Zhang, Y. Liu and J. J. Urban, *ACS Appl. Mater. Inter.*, 2020, **12**, 16922-16929.

29. R. Xue, H. Guo, L. Yue, T. Wang, M. Wang, Q. Li, H. Liu and W. Yang, *New J Chem.*, 2018, **42**, 13726-13731.

30. S. Wei, F. Zhang, W. Zhang, P. Qiang, K. Yu, X. Fu, D. Wu, S. Bi and F. Zhang, *J. Am. Chem. Soc.*, 2019, **141**, 14272-14279.

31. P. Katekomol, J. Roeser, M. Bojdys, J. Weber and A. Thomas, *Chem. Mater.*, 2013, **25**,

1542-1548.

32. Y. Kou, Y. Xu, Z. Guo and D. Jiang, *Angew. Chem. Int. Ed. Engl.*, 2011, **50**, 8753-8757.

33. Z.-Q. Lin, J. Xie, B.-W. Zhang, J.-W. Li, J. Weng, R.-B. Song, X. Huang, H. Zhang, H. Li, Y. Liu, Z. J. Xu, W. Huang and Q. Zhang, *Nano Energy*, 2017, **41**, 117-127.

34. V. Briega-Martos, A. Ferre-Vilaplana, A. de la Peña, J. L. Segura, F. Zamora, J. M. Feliu and E. Herrero, *ACS Catal.*, 2016, **7**, 1015-1024.

35. M. Abel, S. Clair, O. Ourdjini, M. Mossoyan and L. Porte, *J. Am. Chem. Soc.*, 2011, **133**, 1203-1205.